Majorana Corner Modes in a High-Temperature Platform

Zhongbo Yan,[1] Fei Song,[1] and Zhong Wang[1,2,*]
[1]Institute for Advanced Study, Tsinghua University, Beijing 100084, China
[2]Collaborative Innovation Center of Quantum Matter, Beijing 100871, China

(Received 25 March 2018; revised manuscript received 20 June 2018; published 30 August 2018)

We introduce two-dimensional topological insulators in proximity to high-temperature cuprate or iron-based superconductors as high-temperature platforms of Majorana Kramers pairs of zero modes. The proximity-induced pairing at the helical edge state of the topological insulator serves as a Dirac mass, whose sign changes at the sample corner because of the pairing symmetry of high-T_c superconductors. This sign changing naturally creates at each corner a pair of Majorana zero modes protected by time-reversal symmetry. Conceptually, this is a topologically trivial superconductor-based approach for Majorana zero modes. We provide quantitative criteria and suggest candidate materials for this proposal.

DOI: 10.1103/PhysRevLett.121.096803

Majorana zero modes (MZMs) [1–3] have been actively pursued in recent years as building blocks of topological quantum computations [4–11]. These emergent excitations can generate robust ground-state degeneracy, supporting storage of nonlocal qubits robust to local decoherence [12]. Moreover, quantum gates can be implemented by their braiding operations [13–17]. As platforms of MZMs, a variety of realizations of topological superconductors have been proposed, including topological insulators in proximity to conventional superconductors [18–22], semiconductor heterostructures [23–25], cold-atom systems [26–31], and quantum wires [32–35], to name a few; meanwhile, remarkable experimental progress has been witnessed [36–54].

A single MZM entails breaking the time-reversal symmetry (TRS); in contrast, time-reversal-invariant (TRI) topological superconductors [55–62] host Majorana Kramers pairs (MKPs) of zero modes, which are robust in the presence of TRS, and have interesting consequences such as TRS-protected non-Abelian statistics [63–65], TRS as local supersymmetry [55], and novel Kondo effects [66] and Josephson effects [67–71], indicating their potentials in qubit storage or manipulation and other applications. In addition, MKPs can be used as tunable generators of MZMs by breaking the TRS [57,58]. There have been a few interesting proposals for realizing TRI topological superconductors and MKPs [57,58,72–84], though experimental realizations are yet to come.

In this Letter, we show that simple structures of two-dimensional topological insulators (2D TIs) (also known as quantum spin Hall insulators) in proximity to high-temperature superconductors naturally generate MKPs (Fig. 1). Since 2D TIs have been experimentally realized at temperatures as high as 100 K [85,86], this setup can be a high-temperature platform of MKPs. The physical picture can be readily described as follows: The helical edge states of the TI, described as 1D massless Dirac fermions, are gapped out by the induced superconducting gap, which introduces a Dirac mass. Due to the nature of pairing symmetry (say d wave), the induced Dirac mass changes sign at the corner, which generates a MKP as domain-wall excitations.

It is interesting to note that we do not propose here any realization of a TRI topological superconductor. In fact, the helical Majorana edge states of $\mathbb{Z}_2$-nontrivial superconductors cannot be gapped out without breaking TRS. In our setup, the 2D TI with a proximity-induced pairing has gapped edges; therefore it is a $\mathbb{Z}_2$-trivial superconductor. In fact, it has recently been suggested that, as defect modes [87], robust MZMs can be realized in certain topologically trivial superconductors [88,89]. (Particularly, MZMs can in principle be created as corner modes in judiciously designed trivial superconductor junctions [88].) Conceptually, the present Letter generalizes the trivial superconductor-based approach to MKPs, for which ideal candidate materials are available.

d-wave pairing.—As explained above, the key observation comes from the edge states. For concreteness, however, let us start from a lattice model of 2D TIs, in which the proximity-induced pairing is added. The Bogoliubov–de Gennes Hamiltonian is $\hat{H} = \sum_{\mathbf{k}} \Psi_{\mathbf{k}}^\dagger H(\mathbf{k}) \Psi_{\mathbf{k}}$, with $\Psi_{\mathbf{k}} = (c_{a,\mathbf{k}\uparrow}, c_{b,\mathbf{k}\uparrow}, c_{a,\mathbf{k}\downarrow}, c_{b,\mathbf{k}\downarrow}, c_{a,-\mathbf{k}\uparrow}^\dagger, c_{b,-\mathbf{k}\uparrow}^\dagger, c_{a,-\mathbf{k}\downarrow}^\dagger, c_{b,-\mathbf{k}\downarrow}^\dagger)^T$ and

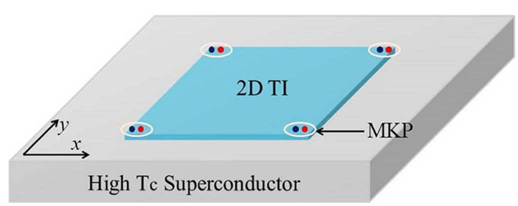

FIG. 1. Schematic illustration. A 2D TI is grown on a d-wave or $s_\pm$-wave high-T_c superconductor. Majorana Kramers pairs (MKPs) of zero modes emerge at the corners of the TI.

$$H(\mathbf{k}) = M(\mathbf{k})\sigma_z\tau_z + A_x \sin k_x \sigma_x s_z + A_y \sin k_y \sigma_y \tau_z + \Delta(\mathbf{k}) s_y \tau_y - \mu\tau_z, \tag{1}$$

where s_i, σ_i, and τ_i are Pauli matrices in the spin $(\uparrow, \downarrow)$, orbital (a, b), and particle-hole spaces, respectively; $M(\mathbf{k}) = m_0 - t_x \cos k_x - t_y \cos k_y$ and $A_{x,y}$ measure the kinetic energy; Δ is the pairing; and μ is the chemical potential. In the following, we will take

$$\Delta(\mathbf{k}) = \Delta_0 + \Delta_x \cos k_x + \Delta_y \cos k_y, \tag{2}$$

which is sufficiently general to model d waves and $s_\pm$ waves. Throughout this Letter, $t_{x,y}$, $A_{x,y}$ are taken to be positive. If the pairing is removed, the Hamiltonian becomes the paradigmatic BHZ model of 2D TIs [85,86,90]. The Hamiltonian has TRS $\mathcal{T}H(\mathbf{k})\mathcal{T}^{-1} = H(-\mathbf{k})$ with $\mathcal{T} = is_y\mathcal{K}$ (where $\mathcal{K}$ is the complex conjugation), and particle-hole symmetry $\mathcal{C}H(\mathbf{k})\mathcal{C}^{-1} = -H(-\mathbf{k})$ with $\mathcal{C} = \tau_x\mathcal{K}$.

We first consider the d-wave pairing that is relevant to cuprate superconductors, which is

$$\Delta_0 = 0, \qquad \Delta_x = -\Delta_y \equiv \Delta_d. \tag{3}$$

The spectra on a cylinder geometry are shown in Fig. 2(a), indicating that the helical edge states of the TI are gapped out by d-wave pairing. From the numerical results for a square geometry [Fig. 2(b)], it is clear that each corner hosts a MKP, whose energy is pinned to zero.

It is interesting to note that, unlike the more familiar vortex or end modes, the Majorana modes here are corner modes. As such, they may be viewed in the framework of recently proposed higher-order topological insulators [91–102] and superconductors [103–106], for which crystal symmetries have been highlighted; the present scheme does not rely sensitively on the crystal symmetries.

We also mention that the bulk of the d-wave superconductor is gapless, and the MKPs may hybridize with these gapless modes. Nevertheless, the MKPs remain observable in scanning tunneling microscopy (STM). Near a MKP, the tunneling conductance displays a zero-bias peak (though broadened by hybridization), which is absent in the usual c-axis tunneling conductance [107] (In other directions, there is zero bias peak [108–114], which is irrelevant in our setup). Later, we also study the $s_\pm$-wave case with an entirely gapped setup, in which case MKPs are the only low-energy modes.

Edge theory.—To gain intuitive understanding, we study the edge theory. To simplify the picture, we take $\mu = 0$ and focus on the continuum model by expanding the lattice Hamiltonian in Eq. (1) to second order around $\mathbf{k} = (0, 0)$:

$$H(\mathbf{k}) = \left(m + \frac{t_x}{2}k_x^2 + \frac{t_y}{2}k_y^2\right)\sigma_z\tau_z + A_x k_x \sigma_x s_z + A_y k_y \sigma_y \tau_z - \frac{1}{2}(\Delta_x k_x^2 + \Delta_y k_y^2) s_y \tau_y, \tag{4}$$

where $\Delta_x + \Delta_y = 0$ has been used for the d wave, and $m = m_0 - t_x - t_y < 0$ is assumed to ensure that the 2D insulator without pairing is in the topologically nontrivial regime. We label the four edges of a square as (I), (II), (III), and (IV) in Fig. 2(b), and we focus on the edge (I) first. We can replace $k_x \to -i\partial_x$ and decompose the Hamiltonian as $H = H_0 + H_p$, in which

$$H_0(-i\partial_x, k_y) = (m - t_x\partial_x^2/2)\sigma_z\tau_z - iA_x\sigma_x s_z \partial_x,$$
$$H_p(-i\partial_x, k_y) = A_y k_y \sigma_y \tau_z + (\Delta_x/2) s_y \tau_y \partial_x^2, \tag{5}$$

where the insignificant k_y^2 term has been omitted. The purpose of this decomposition is to solve H_0 first, and then treat H_p as a perturbation, which is justified when the pairing is relatively small. (This is the case in real samples.)

Solving the eigenvalue equation $H_0\psi_\alpha(x) = E_\alpha\psi_\alpha(x)$ under the boundary condition $\psi_\alpha(0) = \psi_\alpha(+\infty) = 0$, we find four zero-energy solutions, whose forms are

$$\psi_\alpha(x) = \mathcal{N}_x \sin(\kappa_1 x) e^{-\kappa_2 x} e^{ik_y y} \chi_\alpha, \tag{6}$$

with normalization given by $|\mathcal{N}_x|^2 = 4|\kappa_2(\kappa_1^2 + \kappa_2^2)/\kappa_1^2|$. (Here, $\kappa_1 = \sqrt{|(2m/t_x)| - (A_x^2/t_x^2)}$, $\kappa_2 = (A_x/t_x)$. The result remains valid even when κ_1 is imaginary.) The eigenvectors χ_α satisfy $\sigma_y s_z \tau_z \chi_\alpha = -\chi_\alpha$. We can explicitly choose them as

$$\chi_1 = |\sigma_y = -1\rangle \otimes |\uparrow\rangle \otimes |\tau_z = +1\rangle,$$
$$\chi_2 = |\sigma_y = +1\rangle \otimes |\downarrow\rangle \otimes |\tau_z = +1\rangle,$$
$$\chi_3 = |\sigma_y = +1\rangle \otimes |\uparrow\rangle \otimes |\tau_z = -1\rangle,$$
$$\chi_4 = |\sigma_y = -1\rangle \otimes |\downarrow\rangle \otimes |\tau_z = -1\rangle; \tag{7}$$

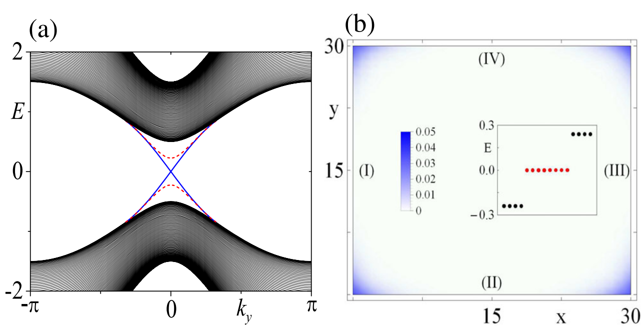

FIG. 2. (a) Energy spectra in a cylinder geometry. $m_0 = 1.5$, $t_x = t_y = 1.0$, $A_x = A_y = 1.0$, $\mu = 0$. Without the pairing, there exist helical edge states traversing the bulk gap (solid blue lines). In the presence of a d-wave pairing ($\Delta_x = -\Delta_y = 0.5$), the edge states become gapped (dashed red lines). The bulk spectra have little difference for these two cases (the zero-pairing case is shown here). (b) The wave function profiles of the four MKPs from solving the real-space lattice Hamiltonian. The sample size is $L_x \times L_y = 30 \times 30$. The inset shows energies near zero, indicating one MKP per corner. (I), (II), (III), and (IV) mark the four edges for use in the edge theory.

then the matrix elements of the perturbation H_p in this basis are

$$H_{\mathrm{I},\alpha\beta}(k_y) = \int_0^{+\infty} dx \psi_\alpha^*(x) H_p(-i\partial_x, k_y)\psi_\beta(x); \quad (8)$$

therefore, the final form of the effective Hamiltonian is

$$H_{\mathrm{I}}(k_y) = -A_y k_y s_z + M_{\mathrm{I}} s_y \tau_y, \quad (9)$$

where

$$M_{\mathrm{I}} = (\Delta_x/2)\int_0^{+\infty} dx \psi_\alpha^*(x)\partial_x^2\psi_\alpha(x) = \Delta_x m/t_x. \quad (10)$$

Similarly, the low-energy effective Hamiltonians for the other three edges are

$$\begin{aligned} H_{\mathrm{II}}(k_x) &= A_x k_x s_z + M_{\mathrm{II}} s_y \tau_y, \\ H_{\mathrm{III}}(k_y) &= A_y k_y s_z + M_{\mathrm{III}} s_y \tau_y, \\ H_{\mathrm{IV}}(k_x) &= -A_x k_x s_z + M_{\mathrm{IV}} s_y \tau_y, \end{aligned} \quad (11)$$

with $M_{\mathrm{II}} = M_{\mathrm{IV}} = \Delta_y m/t_y$, and $M_{\mathrm{III}} = M_{\mathrm{I}}$. To be more transparent, let us take an "edge coordinate" l, which grows in the anticlockwise direction [apparently, l is defined mod $2(L_x + L_y)$]; then the low-energy edge theory becomes

$$H_{\mathrm{edge}} = -iA(l) s_z \partial_l + M(l) s_y \tau_y. \quad (12)$$

The kinetic energy coefficient $A(l)$ and the Dirac mass $M(l)$ are step functions: $A(l) = A_y,\ A_x,\ A_y,\ A_x$ and $M(l) = \Delta_d m/t_x,\ -\Delta_d m/t_y,\ \Delta_d m/t_x,\ -\Delta_d m/t_y$ for (I), (II), (III), and (IV), respectively. At each corner, the $A_{x,y}$ coefficient does not change sign, while the Dirac mass does, which is due to the sign changing in the d-wave pairing: $\Delta_x = -\Delta_y$. Consequently, there is a MKP at each corner (analogous to the Jackiw-Rebbi zero modes [115,116]). For example, at the corner between (I) and (II), we have

$$|\psi_{\mathrm{MKP}}^{\pm}(l)\rangle \propto e^{-\int^l dl' M(l')/A(l')} |s_x = \tau_y = \pm 1\rangle. \quad (13)$$

TRS ensures that these two modes cannot be coupled to generate an energy gap. In essence, the edge theory above can be regarded as two copies of that of Ref. [88], with TRS as the key additional input.

By a similar calculation, one can find that the sign changing in $M(l)$ occurs at a corner when one of the edges has a polar angle within $[-\pi/4, \pi/4]$ and the other within $[\pi/4, 3\pi/4]$ (the gap-maximum direction is taken as the zero polar angle). In Fig. 3(a), the lower corner has a sign changing while the right corner does not, and the existence or absence of MKP is consistent with the edge theory prediction. If one of the edges lies in the $\pi/4$ direction, the edge states become gapless, which also manifests in the numerical spectrum in Fig. 3(b).

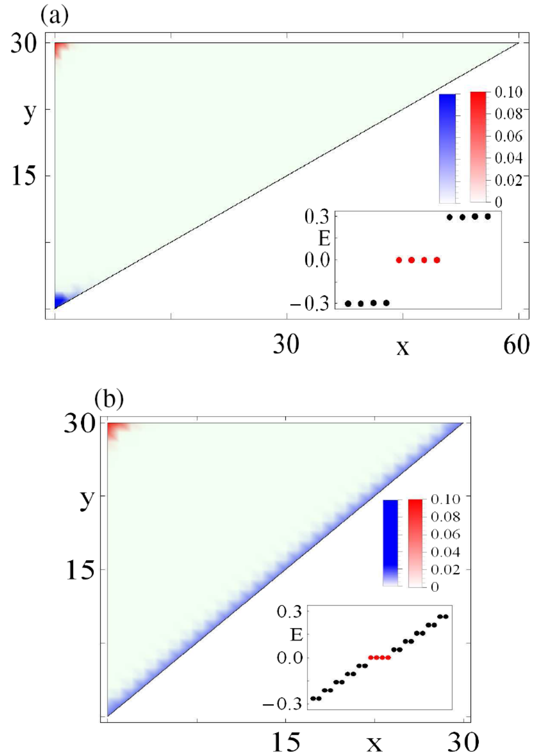

FIG. 3. MKPs in triangle samples. (a) The existence or absence of MKPs depends on the edge directions at the corner, which can be explained in the edge theory. The lower corner has sign change in the edge Dirac mass, while the right corner does not. (b) For a $\pi/4$ angle, the edge Dirac mass vanishes, and the edge states display a gapless feature [see the inset, and compare it to that of (a)]. $m_0 = 1.5$, $t_x = t_y = 2.0$, $A_x = A_y = 2.0$, $\Delta_x = -\Delta_y = 1.0$, $\mu = 0$.

Finally, we mention that cuprate superconductors in proximity to 3D topological insulators have been experimentally studied for the purpose of creating vortex (instead of corner) MZMs [117–120]. In these setups, the 2D topological surface states (instead of the 1D edge states) are the key ingredients.

$s_\pm$-wave pairing.—Now we consider fully gapped $s_\pm$-wave superconductors with sign changing in the pairing. A host of candidates can be found in high-T_c iron-based superconductors [121,122], whose pairings at the Fermi surfaces near the Brillouin zone center and the Brillouin zone boundary both have s-wave nature but with opposite signs. The Fermi surfaces do not cross the pairing nodal rings; therefore, the superconductor is fully gapped. A simple form of $s_\pm$-wave pairing is

$$\Delta(\mathbf{k}) = \Delta_0 - \Delta_1(\cos k_x + \cos k_y), \quad (14)$$

with $0 < \Delta_0 < 2\Delta_1$. The pairing node is $\cos k_x + \cos k_y = \Delta_0/\Delta_1$.

Let us first study the edge theory of TIs. Expanding the Hamiltonian near $\mathbf{k} = (0, 0)$ and taking $\mu = 0$, we have

$$H(\mathbf{k}) = \left(m + \frac{t_x}{2}k_x^2 + \frac{t_y}{2}k_y^2\right)\sigma_z\tau_z + A_x k_x \sigma_x s_z + A_y k_y \sigma_y \tau_z + \left[\Delta_0 - 2\Delta_1 + \frac{\Delta_1}{2}(k_x^2 + k_y^2)\right] s_y \tau_y. \quad (15)$$

Following a similar approach as the previous section, for the edge (I), we decompose the Hamiltonian as $H = H_0 + H_p$, where

$$H_0(-i\partial_x, k_y) = (m - t_x\partial_x^2/2)\sigma_z\tau_z - iA_x\sigma_x s_z \partial_x,$$
$$H_p(-i\partial_x, k_y) = A_y k_y \sigma_y \tau_z + [\Delta_0 - 2\Delta_1 - (\Delta_1/2)\partial_x^2] s_y \tau_y. \quad (16)$$

Similar to the previous section, four zero-energy solutions of H_0 can be found, and H_p takes the following form within this four-dimensional low-energy subspace:

$$H_{\mathrm{I}}(k_y) = -A_y k_y s_z + M_{\mathrm{I}} s_y \tau_y, \quad (17)$$

with $M_{\mathrm{I}} = \int_0^{+\infty} dx \psi_\alpha^*(x)[\Delta_0 - 2\Delta_1 - (\Delta_1/2)\partial_x^2]\psi_\alpha(x) = \Delta_0 - 2\Delta_1 - \Delta_1 m/t_x$. The low-energy effective Hamiltonians for the other three edges take the same forms as in Eq. (11), with Dirac masses $M_{\mathrm{III}} = \Delta_0 - 2\Delta_1 - \Delta_1 m/t_x = M_{\mathrm{I}}$, and $M_{\mathrm{II}} = M_{\mathrm{IV}} = \int_0^{+\infty} dy \psi_\alpha^*(y)[\Delta_0 - 2\Delta_1 - (\Delta_1/2)\partial_y^2]\psi_\alpha(y) = \Delta_0 - 2\Delta_1 - \Delta_1 m/t_y$. Using the edge coordinate l, the effective edge Hamiltonian is the same as in Eq. (12) with the same $A(l)$ but different $M(l)$; namely, $M(l) = -\bar{\Delta}_0 - \Delta_1 m/t_x$, $-\bar{\Delta}_0 - \Delta_1 m/t_y$, $-\bar{\Delta}_0 - \Delta_1 m/t_x$, and $-\bar{\Delta}_0 - \Delta_1 m/t_y$ for (I), (II), (III), and (IV), respectively, where we have defined $\bar{\Delta}_0 = 2\Delta_1 - \Delta_0$.

To have MKPs at each corner, the sign of the Dirac mass $M(l)$ must change from an edge to its adjacent, which leads to the following criterion:

$$(\bar{\Delta}_0 + \Delta_1 m/t_x)(\bar{\Delta}_0 + \Delta_1 m/t_y) < 0. \quad (18)$$

Let us define $R_s \equiv \sqrt{2\bar{\Delta}_0/\Delta_1}$, whose physical meaning is the radius of the ring of the pairing node, across which the pairing changes sign, and $R_x \equiv \sqrt{-2m/t_x}$ and $R_y \equiv \sqrt{-2m/t_y}$, whose meanings are the two semiaxes of the ellipse determined by $m + (t_x/2)k_x^2 + (t_y/2)k_y^2 = 0$ (i.e., the "band-inversion ring" of TI, where the sign of the σ_z term changes). The mode existence criterion in Eq. (18) (for $\mu = 0$) becomes

$$(R_s - R_x)(R_s - R_y) < 0, \quad (19)$$

which means that the band-inversion ring has to cross the pairing nodal ring [Fig. 4(a)]. Although derived from the continuum model, Eq. (19) is quite accurate according to our lattice-model numerical results [123]. Intuitively, the low-energy edge modes come mainly from states near the band inversion (where the bulk states have the lowest energies) and inherit the sign of pairing there. When the two rings cross, the pairing sign at band inversion is opposite at two adjacent edges, which supports MKPs. We emphasize that the TI has to be anisotropic in the x and y directions to satisfy Eq. (19) ($R_x \neq R_y$), which is the case for the high-transition-temperature TI WTe_2 [85]. In Fig. 4(b), one finds the existence of MKP when Eq. (19) is satisfied. Including a modest chemical potential with a Fermi surface is innocuous [Fig. 4(c)], as the Fermi surface can be gapped out by the induced pairing as long as it does not cross the pairing node. A $(m, \Delta_0/\Delta_1, \mu)$ phase diagram is shown in Fig. 4(d).

So far, we have not discussed disorders. We have numerically confirmed that usual disorders such as on-site random potential does not destroy the MKPs [123]. In addition, our proposal does not require atomically precise edges. Modest edge imperfections do not affect the MKPs, because they are pinned to zero energy by particle-hole symmetry; "big" edge imperfections just create new corners that host their own MKPs, which offer more opportunity to observe MKPs [123].

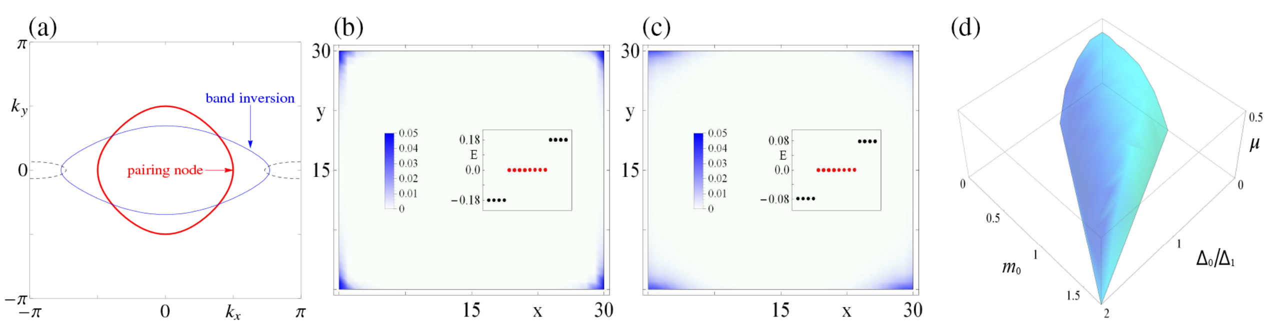

FIG. 4. (a) The pairing nodal ring (red thick line) and band-inversion ring (blue thin line) for $m_0 = 1.0$. The dashed line denotes the Fermi surface for $\mu = 0.3$. (b), (c) The wave function profiles of MKPs for (b) $\mu = 0$ and (c) $\mu = 0.3$, with $\Delta_0 = \Delta_1 = 0.4$. (d) $(m_0, \Delta_0/\Delta_1, \mu)$ phase diagram with fixed $\Delta_1 = 0.4$. Corner modes are found in the surface-enclosed region. Common parameters: $t_x = A_x = 0.4$, $t_y = A_y = 1.3$.

Finally, it is useful to mention that, in both the d-wave and $s_{\pm}$-wave cases, a single MZM can be created from the MKP at the corner by killing one mode in the pair. Apparently, TRS must be broken. For example, it can be achieved by adding an in-plane magnetic field with an appropriate magnitude. The physical picture is most transparent in the edge theory (see the Supplemental Material for details [123]).

Experimental estimations.—For concreteness, let us focus on the high-temperature $s_{\pm}$-wave iron-based superconductors. As emphasized above, in the $s_{\pm}$-wave case the TI band structure is required to be anisotropic in the x and y directions [due to Eq. (19)]. Notably, the monolayer WTe_2, which has recently been confirmed as a high-temperature TI in experiments [85] (up to 100 K), has the desired band structure [86]. According to the $\mathbf{k}\cdot\mathbf{p}$ model in Ref. [86], we fit the parameters to be $R_x = 0.41$ Å^{-1}, $R_y = 0.15$ Å^{-1} (details are given in the Supplemental Material [123]). The reciprocal lattice vectors of WTe_2 along the x and y directions are $G_x \simeq 1.0$ Å^{-1} and $G_y \simeq 1.8$ Å^{-1}. Thus, the band-inversion ring reaches close to the Brillouin zone boundary in the x direction, while it stays close to the zone center in the y direction, resembling the advantageous shape of the band-inversion ring in Fig. 4(a). Although an accurate estimation of the magnitude of the induced pairing gap is not available, we note that cuprate superconductors can induce a gap of tens of milli-electron-volts at the surface states of topological insulators [117,118]; presumably a similar order of magnitude can be expected in the present setup. Therefore, among other options, a setup composed of a WTe_2 monolayer in proximity to high-T_c iron-based superconductors is promising for the present proposal. A WTe_2 monolayer in proximity to cuprate superconductors is also promising.

Conclusions.—We have shown that a 2D TI with proximity-induced d-wave or $s_{\pm}$-wave pairing, though being topologically trivial as a TRI superconductor, is a promising candidate of a high-temperature platform for realizing robust Majorana corner modes. We provide quantitative criteria for this proposal. This Letter may also stimulate further studies of topologically trivial superconductor-based Majorana modes.

We would like to thank Wei Li for helpful discussions. This work is supported by NSFC (Grant No. 11674189). Z. Y. is supported in part by the China Postdoctoral Science Foundation (Grant No. 2016M590082).

Note added.—Recently, there appeared a related preprint [127] that focuses on the $s_{\pm}$-wave case.

*wangzhongemail@gmail.com

[1] N. Read and D. Green, Paired states of fermions in two dimensions with breaking of parity and time-reversal symmetries and the fractional quantum Hall effect, Phys. Rev. B **61**, 10267 (2000).
[2] G. E. Volovik, Fermion zero modes on vortices in chiral superconductors, JETP Lett. **70**, 609 (1999).
[3] A. Yu Kitaev, Unpaired Majorana fermions in quantum wires, Phys. Usp. **44**, 131 (2001).
[4] J. Alicea, New directions in the pursuit of Majorana fermions in solid state systems, Rep. Prog. Phys. **75**, 076501 (2012).
[5] C. W. J. Beenakker, Search for Majorana fermions in superconductors, Annu. Rev. Condens. Matter Phys. **4**, 113 (2013).
[6] T. D. Stanescu and S. Tewari, Majorana fermions in semiconductor nanowires: Fundamentals, modeling, and experiment, J. Phys. Condens. Matter **25**, 233201 (2013).
[7] M. Leijnse and K. Flensberg, Introduction to topological superconductivity and Majorana fermions, Semicond. Sci. Technol. **27**, 124003 (2012).
[8] S. R. Elliott and M. Franz, Colloquium: Majorana fermions in nuclear, particle, and solid-state physics, Rev. Mod. Phys. **87**, 137 (2015).
[9] S. Das Sarma, M. Freedman, and C. Nayak, Majorana zero modes and topological quantum computation, npj Quantum Inf. **1**, 15001 (2015).
[10] M. Sato and S. Fujimoto, Majorana fermions and topology in superconductors, J. Phys. Soc. Jpn. **85**, 072001 (2016).
[11] R. Aguado, Majorana quasiparticles in condensed matter, Riv. Nuovo Cimento **40**, 523 (2017).
[12] C. Nayak, S. H. Simon, A. Stern, M. Freedman, and S. Das Sarma, Non-Abelian anyons and topological quantum computation, Rev. Mod. Phys. **80**, 1083 (2008).
[13] G. Moore and N. Read, Non-Abelions in the fractional quantum Hall effect, Nucl. Phys. **B360**, 362 (1991).
[14] X.-G. Wen, Non-Abelian Statistics in the Fractional Quantum Hall States, Phys. Rev. Lett. **66**, 802 (1991).
[15] D. A. Ivanov, Non-Abelian Statistics of Half-Quantum Vortices in p-Wave Superconductors, Phys. Rev. Lett. **86**, 268 (2001).
[16] C. Nayak and F. Wilczek, $2n$-quasihole states realize 2^{n-1}-dimensional spinor braiding statistics in paired quantum Hall states, Nucl. Phys. **B479**, 529 (1996).
[17] S. Das Sarma, M. Freedman, and C. Nayak, Topologically Protected Qubits from a Possible Non-Abelian Fractional Quantum Hall State, Phys. Rev. Lett. **94**, 166802 (2005).
[18] L. Fu and C. L. Kane, Superconducting Proximity Effect and Majorana Fermions at the Surface of a Topological Insulator, Phys. Rev. Lett. **100**, 096407 (2008).
[19] X.-L. Qi, T. L. Hughes, and S.-C. Zhang, Chiral topological superconductor from the quantum Hall state, Phys. Rev. B **82**, 184516 (2010).
[20] A. R. Akhmerov, J. Nilsson, and C. W. J. Beenakker, Electrically Detected Interferometry of Majorana Fermions in a Topological Insulator, Phys. Rev. Lett. **102**, 216404 (2009).
[21] K. T. Law, P. A. Lee, and T. K. Ng, Majorana Fermion Induced Resonant Andreev Reflection, Phys. Rev. Lett. **103**, 237001 (2009).
[22] S. B. Chung, X.-L. Qi, J. Maciejko, and S.-C. Zhang, Conductance and noise signatures of Majorana backscattering, Phys. Rev. B **83**, 100512 (2011).
[23] J. D. Sau, R. M. Lutchyn, S. Tewari, and S. Das Sarma, Generic New Platform for Topological Quantum

Computation Using Semiconductor Heterostructures, Phys. Rev. Lett. **104**, 040502 (2010).

[24] J. Alicea, Majorana fermions in a tunable semiconductor device, Phys. Rev. B **81**, 125318 (2010).

[25] G. Xu, J. Wang, B. Yan, and X.-L. Qi, Topological superconductivity at the edge of transition-metal dichalcogenides, Phys. Rev. B **90**, 100505 (2014).

[26] L. Jiang, T. Kitagawa, J. Alicea, A. R. Akhmerov, D. Pekker, G. Refael, J. I. Cirac, E. Demler, M. D. Lukin, and P. Zoller, Majorana Fermions in Equilibrium and in Driven Cold-Atom Quantum Wires, Phys. Rev. Lett. **106**, 220402 (2011).

[27] S. Diehl, E. Rico, M. A. Baranov, and P. Zoller, Topology by dissipation in atomic quantum wires, Nat. Phys. **7**, 971 (2011).

[28] M. Sato, Y. Takahashi, and S. Fujimoto, Non-Abelian Topological Order in s-Wave Superfluids of Ultracold Fermionic Atoms, Phys. Rev. Lett. **103**, 020401 (2009).

[29] C. Zhang, S. Tewari, R. M. Lutchyn, and S. Das Sarma, $p_x + ip_y$ Superfluid from s-Wave Interactions of Fermionic Cold Atoms, Phys. Rev. Lett. **101**, 160401 (2008).

[30] S. Tewari, S. Das Sarma, C. Nayak, C. Zhang, and P. Zoller, Quantum Computation Using Vortices and Majorana Zero Modes of a $p_x + ip_y$ Superfluid of Fermionic Cold Atoms, Phys. Rev. Lett. **98**, 010506 (2007).

[31] X.-J. Liu, K. T. Law, and T. K. Ng, Realization of 2D Spin-Orbit Interaction and Exotic Topological Orders in Cold Atoms, Phys. Rev. Lett. **112**, 086401 (2014).

[32] Y. Oreg, G. Refael, and F. von Oppen, Helical Liquids and Majorana Bound States in Quantum Wires, Phys. Rev. Lett. **105**, 177002 (2010).

[33] R. M. Lutchyn, J. D. Sau, and S. Das Sarma, Majorana Fermions and a Topological Phase Transition in Semiconductor-Superconductor Heterostructures, Phys. Rev. Lett. **105**, 077001 (2010).

[34] M. M. Vazifeh and M. Franz, Self-Organized Topological State with Majorana Fermions, Phys. Rev. Lett. **111**, 206802 (2013).

[35] A. Cook and M. Franz, Majorana fermions in a topological-insulator nanowire proximity-coupled to an s-wave superconductor, Phys. Rev. B **84**, 201105 (2011).

[36] V. Mourik, K. Zuo, S. M. Frolov, S. R. Plissard, E. P. A. M. Bakkers, and L. P. Kouwenhoven, Signatures of Majorana fermions in hybrid superconductor-semiconductor nanowire devices, Science **336**, 1003 (2012).

[37] S. Nadj-Perge, I. K. Drozdov, J. Li, H. Chen, S. Jeon, J. Seo, A. H. MacDonald, B. A. Bernevig, and A. Yazdani, Observation of Majorana fermions in ferromagnetic atomic chains on a superconductor, Science **346**, 602 (2014).

[38] L. P. Rokhinson, X. Liu, and J. K. Furdyna, The fractional ac Josephson effect in a semiconductor-superconductor nanowire as a signature of Majorana particles, Nat. Phys. **8**, 795 (2012).

[39] M. T. Deng, C. L. Yu, G. Y. Huang, M. Larsson, P. Caroff, and H. Q. Xu, Anomalous zero-bias conductance peak in a Nb-InSb nanowire-Nb hybrid device, Nano Lett. **12**, 6414 (2012).

[40] A. Das, Y. Ronen, Y. Most, Y. Oreg, M. Heiblum, and H. Shtrikman, Zero-bias peaks and splitting in an Al-InAs nanowire topological superconductor as a signature of Majorana fermions, Nat. Phys. **8**, 887 (2012).

[41] A. D. K. Finck, D. J. Van Harlingen, P. K. Mohseni, K. Jung, and X. Li, Anomalous Modulation of a Zero-Bias Peak in a Hybrid Nanowire-Superconductor Device, Phys. Rev. Lett. **110**, 126406 (2013).

[42] H. O. H. Churchill, V. Fatemi, K. Grove-Rasmussen, M. T. Deng, P. Caroff, H. Q. Xu, and C. M. Marcus, Superconductor-nanowire devices from tunneling to the multichannel regime: Zero-bias oscillations and magnetoconductance crossover, Phys. Rev. B **87**, 241401 (2013).

[43] Y.-F. Lv, W.-L. Wang, Y.-M. Zhang, H. Ding, W. Li, L. Wang, K. He, C.-L. Song, X.-C. Ma, and Q.-K. Xue, Experimental observation of topological superconductivity and Majorana zero modes on β-Bi_2Pd thin films, Sci. Bulletin **62**, 852 (2017).

[44] M.-X. Wang, C. Liu, J.-P. Xu, F. Yang, L. Miao, M.-Y. Yao, C. L. Gao, C. Shen, X. Ma, X. Chen *et al.*, The coexistence of superconductivity and topological order in the Bi_2Se_3 thin films, Science **336**, 52 (2012).

[45] Z. F. Wang, H. Zhang, D. Liu, C. Liu, C. Tang, C. Song, Y. Zhong, J. Peng, F. Li, C. Nie, L. Wang, X. J. Zhou, X. Ma, Q. K. Xue, and F. Liu, Topological edge states in a high-temperature superconductor $FeSe/SrTiO_3(001)$ film, Nat. Mater. **15**, 968 (2016).

[46] S. M. Albrecht, A. P. Higginbotham, M. Madsen, F. Kuemmeth, T. S. Jespersen, J. Nygård, P. Krogstrup, and C. M. Marcus, Exponential protection of zero modes in Majorana islands, Nature (London) **531**, 206 (2016).

[47] M. T. Deng, S. Vaitiekėnas, E. B. Hansen, J. Danon, M. Leijnse, K. Flensberg, J. Nygård, P. Krogstrup, and C. M. Marcus, Majorana bound state in a coupled quantum-dot hybrid-nanowire system, Science **354**, 1557 (2016).

[48] R. Pawlak, M. Kisiel, J. Klinovaja, T. Meier, S. Kawai, T. Glatzel, D. Loss, and E. Meyer, Probing atomic structure and Majorana wavefunctions in mono-atomic Fe chains on superconducting Pb surface, npj Quantum Inf. **2**, 16035 (2016).

[49] J.-P. Xu, M.-X. Wang, Z. L. Liu, J.-F. Ge, X. Yang, C. Liu, Z. A. Xu, D. Guan, C. L. Gao, D. Qian, Y. Liu, Q.-H. Wang, F.-C. Zhang, Q.-K. Xue, and J.-F. Jia, Experimental Detection of a Majorana Mode in the Core of a Magnetic Vortex inside a Topological Insulator-Superconductor $Bi_2Te_3/NbSe_2$ Heterostructure, Phys. Rev. Lett. **114**, 017001 (2015).

[50] H.-H. Sun, K.-W. Zhang, L.-H. Hu, C. Li, G.-Y. Wang, H.-Y. Ma, Z.-A. Xu, C.-L. Gao, D.-D. Guan, Y.-Y. Li, C. Liu, D. Qian, Y. Zhou, L. Fu, S.-C. Li, F.-C. Zhang, and J.-F. Jia, Majorana Zero Mode Detected with Spin Selective Andreev Reflection in the Vortex of a Topological Superconductor, Phys. Rev. Lett. **116**, 257003 (2016).

[51] Q. L. He, L. Pan, A. L. Stern, E. Burks, X. Che, G. Yin, J. Wang, B. Lian, Q. Zhou, E. S. Choi, K. Murata, X. Kou, T. Nie, Q. Shao, Y. Fan, S.-C. Zhang, K. Liu, J. Xia, and K. L. Wang, Chiral Majorana Edge State in a Quantum Anomalous Hall Insulator–Superconductor Structure, Science **357**, 294 (2017).

[52] H. Zhang, C.-X. Liu, S. Gazibegovic, D. Xu, J. A. Logan, G. Wang, N. van Loo, J. D. S. Bommer, M. W. A. de Moor,

D. Car *et al.*, Quantized Majorana conductance, Nature (London) **556**, 74 (2018).
[53] P. Zhang, K. Yaji, T. Hashimoto, Y. Ota, T. Kondo, K. Okazaki, Z. Wang, J. Wen, G. D. Gu, H. Ding *et al.*, Observation of topological superconductivity on the surface of an iron-based superconductor, Science **03**, 4596 (2018).
[54] D. Wang, L. Kong, P. Fan, H. Chen, Y. Sun, S. Du, J. Schneeloch, R. D. Zhong, G. D. Gu, L. Fu *et al.*, Observation of Pristine Majorana Bound State in Iron-Based Superconductor, Science, eaao1797 (2018).
[55] X.-L. Qi, T. L. Hughes, S. Raghu, and S.-C. Zhang, Time-Reversal-Invariant Topological Superconductors and Superfluids in Two and Three Dimensions, Phys. Rev. Lett. **102**, 187001 (2009).
[56] X.-L. Qi, T. L. Hughes, and S.-C. Zhang, Topological invariants for the Fermi surface of a time-reversal-invariant superconductor, Phys. Rev. B **81**, 134508 (2010).
[57] F. Zhang, C. L. Kane, and E. J. Mele, Time-Reversal-Invariant Topological Superconductivity and Majorana Kramers Pairs, Phys. Rev. Lett. **111**, 056402 (2013).
[58] C. L. M. Wong and K. T. Law, Majorana Kramers doublets in $d_{x^2-y^2}$-wave superconductors with Rashba spin-orbit coupling, Phys. Rev. B **86**, 184516 (2012).
[59] M. Sato, Topological odd-parity superconductors, Phys. Rev. B **81**, 220504 (2010).
[60] F. Zhang, C. L. Kane, and E. J. Mele, Topological Mirror Superconductivity, Phys. Rev. Lett. **111**, 056403 (2013).
[61] L. Fu and E. Berg, Odd-Parity Topological Superconductors: Theory and Application to $Cu_xBi_2Se_3$, Phys. Rev. Lett. **105**, 097001 (2010).
[62] A. Haim, E. Berg, K. Flensberg, and Y. Oreg, No-go theorem for a time-reversal invariant topological phase in noninteracting systems coupled to conventional superconductors, Phys. Rev. B **94**, 161110 (2016).
[63] X.-J. Liu, C. L. M. Wong, and K. T. Law, Non-Abelian Majorana Doublets in Time-Reversal-Invariant Topological Superconductors, Phys. Rev. X **4**, 021018 (2014).
[64] F. Zhang and C. L. Kane, Anomalous topological pumps and fractional Josephson effects, Phys. Rev. B **90**, 020501 (2014).
[65] P. Gao, Y.-P. He, and X.-J. Liu, Symmetry-protected non-Abelian braiding of Majorana Kramers pairs, Phys. Rev. B **94**, 224509 (2016).
[66] Z.-q. Bao and F. Zhang, Topological Majorana Two-Channel Kondo Effect, Phys. Rev. Lett. **119**, 187701 (2017).
[67] F. Zhang and C. L. Kane, Time-Reversal-Invariant Z_4 Fractional Josephson Effect, Phys. Rev. Lett. **113**, 036401 (2014).
[68] C. P. Orth, R. P. Tiwari, T. Meng, and T. L. Schmidt, Non-Abelian parafermions in time-reversal-invariant interacting helical systems, Phys. Rev. B **91**, 081406 (2015).
[69] C. Schrade, A. A. Zyuzin, J. Klinovaja, and D. Loss, Proximity-Induced π Josephson Junctions in Topological Insulators and Kramers Pairs of Majorana Fermions, Phys. Rev. Lett. **115**, 237001 (2015).
[70] C. Schrade and L. Fu, Parity-Controlled 2π Josephson Effect Mediated by Majorana Kramers Pairs, Phys. Rev. Lett. **120**, 267002 (2018).
[71] A. Camjayi, L. Arrachea, A. Aligia, and F. von Oppen, Fractional Spin and Josephson Effect in Time-Reversal-Invariant Topological Superconductors, Phys. Rev. Lett. **119**, 046801 (2017).
[72] A. Keselman, L. Fu, A. Stern, and E. Berg, Inducing Time-Reversal-Invariant Topological Superconductivity and Fermion Parity Pumping in Quantum Wires, Phys. Rev. Lett. **111**, 116402 (2013).
[73] S. Nakosai, J. C. Budich, Y. Tanaka, B. Trauzettel, and N. Nagaosa, Majorana Bound States and Nonlocal Spin Correlations in a Quantum Wire on an Unconventional Superconductor, Phys. Rev. Lett. **110**, 117002 (2013).
[74] S. Nakosai, Y. Tanaka, and N. Nagaosa, Topological Superconductivity in Bilayer Rashba System, Phys. Rev. Lett. **108**, 147003 (2012).
[75] J. Wang, Y. Xu, and S.-C. Zhang, Two-dimensional time-reversal-invariant topological superconductivity in a doped quantum spin-Hall insulator, Phys. Rev. B **90**, 054503 (2014).
[76] A. Haim, A. Keselman, E. Berg, and Y. Oreg, Time-reversal-invariant topological superconductivity induced by repulsive interactions in quantum wires, Phys. Rev. B **89**, 220504 (2014).
[77] J. Klinovaja, A. Yacoby, and D. Loss, Kramers pairs of Majorana fermions and parafermions in fractional topological insulators, Phys. Rev. B **90**, 155447 (2014).
[78] F. Yang, C.-C. Liu, Y.-Z. Zhang, Y. Yao, and D.-H. Lee, Time-reversal-invariant topological superconductivity in n-doped BiH, Phys. Rev. B **91**, 134514 (2015).
[79] F. Trani, G. Campagnano, A. Tagliacozzo, and P. Lucignano, High critical temperature nodal superconductors as building block for time-reversal invariant topological superconductivity, Phys. Rev. B **94**, 134518 (2016).
[80] J. Li, W. Pan, B. A. Bernevig, and R. M. Lutchyn, Detection of Majorana Kramers Pairs Using a Quantum Point Contact, Phys. Rev. Lett. **117**, 046804 (2016).
[81] F. Wu and I. Martin, Majorana Kramers pair in a nematic vortex, Phys. Rev. B **95**, 224503 (2017).
[82] C. Reeg, C. Schrade, J. Klinovaja, and D. Loss, DIII topological superconductivity with emergent time-reversal symmetry, Phys. Rev. B **96**, 161407 (2017).
[83] J. Wang, Electrically tunable topological superconductivity and Majorana fermions in two dimensions, Phys. Rev. B **94**, 214502 (2016).
[84] H. Hu, F. Zhang, and C. Zhang, Majorana doublets, flat bands, and Dirac nodes in s-wave superfluids, arXiv:1710.06388.
[85] S. Wu, V. Fatemi, Q. D. Gibson, K. Watanabe, T. Taniguchi, R. J. Cava, and P. Jarillo-Herrero, Observation of the quantum spin Hall effect up to 100 kelvin in a monolayer crystal, Science **359**, 76 (2018).
[86] X. Qian, J. Liu, L. Fu, and J. Li, Quantum spin Hall effect in two-dimensional transition metal dichalcogenides, Science **346**, 1344 (2014).
[87] J. C. Y. Teo and C. L. Kane, Topological defects and gapless modes in insulators and superconductors, Phys. Rev. B **82**, 115120 (2010).
[88] Z. Yan, R. Bi, and Z. Wang, Majorana Zero Modes Protected by a Hopf Invariant in Topologically Trivial Superconductors, Phys. Rev. Lett. **118**, 147003 (2017).

[89] C. Chan, L. Zhang, T. F. J. Poon, Y.-P. He, Y.-Q. Wang, and X.-J. Liu, Generic Theory for Majorana Zero Modes in 2D Superconductors, Phys. Rev. Lett. **119**, 047001 (2017).

[90] B. A. Bernevig, T. L. Hughes, and S. C. Zhang, Quantum spin Hall effect and topological phase transition in HgTe quantum wells, Science **314**, 1757 (2006).

[91] W. A. Benalcazar, B. A. Bernevig, and T. L. Hughes, Quantized electric multipole insulators, Science **357**, 61 (2017).

[92] F. Schindler, A. M. Cook, M. G. Vergniory, Z. Wang, S. S. P. Parkin, B. A. Bernevig, and T. Neupert, Higher-order topological insulators, Sci. Adv. **4**, eaat0346 (2018).

[93] F. Zhang, C. L. Kane, and E. J. Mele, Surface State Magnetization and Chiral Edge States on Topological Insulators, Phys. Rev. Lett. **110**, 046404 (2013).

[94] W. A. Benalcazar, B. A. Bernevig, and T. L. Hughes, Electric multipole moments, topological multipole moment pumping, and chiral hinge states in crystalline insulators, Phys. Rev. B **96**, 245115 (2017).

[95] Z. Song, Z. Fang, and C. Fang, $(d-2)$-Dimensional Edge States of Rotation Symmetry Protected Topological States, Phys. Rev. Lett. **119**, 246402 (2017).

[96] J. Langbehn, Y. Peng, L. Trifunovic, F. von Oppen, and P. W. Brouwer, Reflection-Symmetric Second-Order Topological Insulators and Superconductors, Phys. Rev. Lett. **119**, 246401 (2017).

[97] Y. Peng, Y. Bao, and F. von Oppen, Boundary Green functions of topological insulators and superconductors, Phys. Rev. B **95**, 235143 (2017).

[98] S. Imhof, C. Berger, F. Bayer, J. Brehm, L. Molenkamp, T. Kiessling, F. Schindler, C. H. Lee, M. Greiter, T. Neupert, and R. Thomale, Topolectrical circuit realization of topological corner modes, arXiv:1708.03647.

[99] M. Serra-Garcia, V. Peri, R. Süsstrunk, O. R. Bilal, T. Larsen, L. G. Villanueva, and S. D. Huber, Observation of a phononic quadrupole topological insulator, Nature **555**, 342 (2018).

[100] F. Schindler, Z. Wang, M. G. Vergniory, A. M. Cook, A. Murani, S. Sengupta, A. Y. Kasumov, R. Deblock, S. Jeon, I. Drozdov, H. Bouchiat, S. Guéron, A. Yazdani, B. A. Bernevig, and T. Neupert, Higher-order topology in bismuth, arXiv:1802.02585.

[101] M. Ezawa, Higher-Order Topological Insulators and Semimetals on the Breathing Kagome and Pyrochlore Lattices, Phys. Rev. Lett. **120**, 026801 (2018).

[102] C. W. Peterson, W. A. Benalcazar, T. L. Hughes, and G. Bahl, A quantized microwave quadrupole insulator with topologically protected corner states, Nature (London) **555**, 346 (2018).

[103] M. Geier, L. Trifunovic, M. Hoskam, and P. W. Brouwer, Second-order topological insulators and superconductors with an order-two crystalline symmetry, Phys. Rev. B **97**, 205135 (2018).

[104] X. Zhu, Tunable Majorana corner states in a two-dimensional second-order topological superconductor induced by magnetic fields, Phys. Rev. B **97**, 205134 (2018).

[105] E. Khalaf, Higher-order topological insulators and superconductors protected by inversion symmetry, Phys. Rev. B **97**, 205136 (2018).

[106] H. Shapourian, Y. Wang, and S. Ryu, Topological crystalline superconductivity and second-order topological superconductivity in nodal-loop materials, Phys. Rev. B **97**, 094508 (2018).

[107] Ø. Fischer, M. Kugler, I. Maggio-Aprile, C. Berthod, and C. Renner, Scanning tunneling spectroscopy of high-temperature superconductors, Rev. Mod. Phys. **79**, 353 (2007).

[108] S. Kashiwaya, Y. Tanaka, M. Koyanagi, H. Takashima, and K. Kajimura, Origin of zero-bias conductance peaks in high-t_c superconductors, Phys. Rev. B **51**, 1350 (1995).

[109] S. Sinha and K.-W. Ng, Zero Bias Conductance Peak Enhancement in $Bi_2Sr_2CaCu_2O_8/Pb$ Tunneling Junctions, Phys. Rev. Lett. **80**, 1296 (1998).

[110] Y. Tanaka and S. Kashiwaya, Theory of Tunneling Spectroscopy of d-Wave Superconductors, Phys. Rev. Lett. **74**, 3451 (1995).

[111] S. Ryu and Y. Hatsugai, Topological Origin of Zero-Energy Edge States in Particle-Hole Symmetric Systems, Phys. Rev. Lett. **89**, 077002 (2002).

[112] I. Shigeta, F. Ichikawa, and T. Aomine, Temperature dependence of zero-bias conductance peak in $Bi_2Sr_2CaCu_2O_{8+}$-SiO-Ag planar tunnel junctions, Physica (Amsterdam) **378C**, 316 (2002).

[113] F. Giubileo, A. Jossa, F. Bobba, A. I. Akimenko, G. Malandrino, L. M. S. Perdicaro, I. L. Fragala, and A. M. Cucolo, Study of Andreev reflections in $Tl_2Ba_2CaCu_2O_8/Ag$ interfaces, Physica (Amsterdam) **367C**, 170 (2002).

[114] J.-T. Kao, S.-M. Huang, C.-Y. Mou, and C. C. Tsuei, Tunneling spectroscopy and Majorana modes emergent from topological gapless phases in high-T_c cuprate superconductors, Phys. Rev. B **91**, 134501 (2015).

[115] R. Jackiw and C. Rebbi, Solitons with fermion number $1/2$, Phys. Rev. D **13**, 3398 (1976).

[116] D.-H. Lee, G.-M. Zhang, and T. Xiang, Edge Solitons of Topological Insulators and Fractionalized Quasiparticles in Two Dimensions, Phys. Rev. Lett. **99**, 196805 (2007).

[117] E. Wang, H. Ding, A. V. Fedorov, W. Yao, Z. Li, Y.-F. Lv, K. Zhao, L.-G. Zhang, Z. Xu, J. Schneeloch, R. Zhong, S.-H. Ji, L. Wang, K. He, X. Ma, G. Gu, H. Yao, Q.-K. Xue, X. Chen, and S. Zhou, Fully gapped topological surface states in Bi_2Se_3 films induced by a d-wave high-temperature superconductor, Nat. Phys. **9**, 621 (2013).

[118] P. Zareapour, A. Hayat, S. Y. F. Zhao, M. Kreshchuk, A. Jain, D. C. Kwok, N. Lee, S.-W. Cheong, Z. Xu, A. Yang, G. D. Gu, S. Jia, R. J. Cava, and K. S. Burch, Proximity-induced high-temperature superconductivity in the topological insulators Bi_2Se_3 and Bi_2Te_3, Nat. Commun. **3**, 1056 (2012).

[119] Z.-X. Li, C. Chan, and H. Yao, Realizing Majorana zero modes by proximity effect between topological insulators and d-wave high-temperature superconductors, Phys. Rev. B **91**, 235143 (2015).

[120] L. Ortiz, S. Varona, O. Viyuela, and M. A. Martin-Delgado, Localization and oscillations of Majorana fermions in a two-dimensional electron gas coupled with d-wave superconductors, Phys. Rev. B **97**, 064501 (2018).

[121] G. R. Stewart, Superconductivity in iron compounds, Rev. Mod. Phys. **83**, 1589 (2011).

[122] P. J. Hirschfeld, M. M. Korshunov, and I. I. Mazin, Gap symmetry and structure of Fe-based superconductors, Rep. Prog. Phys. **74**, 124508 (2011).

[123] See Supplemental Material at http://link.aps.org/supplemental/10.1103/PhysRevLett.121.096803 for details of calculations and experimental estimations, which includes Refs. [124–126].

[124] H. Won and K. Maki, *d*-wave superconductor as a model of high-t_c superconductors, Phys. Rev. B **49**, 1397 (1994).

[125] M. Kugler, G. Levy de Castro, E. Giannini, A. Piriou, A. A. Manuel, C. Hess, and Ø. Fischer, Scanning tunneling spectroscopy on $Bi_2Sr_2Ca_2Cu_3O_{10+\delta}$ single crystals, J. Phys. Chem. Solids **67**, 353 (2006); spectroscopies in Novel Superconductors 2004.

[126] J. E. Hoffman, Spectroscopic scanning tunneling microscopy insights into Fe-based superconductors, Rep. Prog. Phys. **74**, 124513 (2011).

[127] Q. Wang, C.-C. Liu, Y.-M. Lu, and F. Zhang, High-temperature Majorana corner states, arXiv:1804.04711.